Title
Defect-Enhanced Polarization Switching in the Improper Ferroelectric LuFeO3

Journal
Advanced Materials, 32(23)

ISSN
0935-9648

Authors
Barrozo, Petrucio
Småbråten, Didrik René
Tang, Yun-Long
et al.

Publication Date
2020-06-01

DOI
10.1002/adma.202000508

Peer reviewed

Defect-Enhanced Polarization Switching in the Improper Ferroelectric $LuFeO_3$

Petrucio Barrozo, Didrik René Småbråten, Yun-Long Tang, Bhagwati Prasad, Sahar Saremi, Rustem Ozgur, Vishal Thakare, Rachel A. Steinhardt, Megan E. Holtz, Vladimir Alexandru Stoica, Lane W. Martin, Darrel G. Schlom, Sverre Magnus Selbach, and Ramamoorthy Ramesh**

Results of switching behavior of the improper ferroelectric $LuFeO_3$ are presented. Using a model set of films prepared under controlled chemical and growth-rate conditions, it is shown that defects can reduce the quasi-static switching voltage by up to 40% in qualitative agreement with first-principles calculations. Switching studies show that the coercive field has a stronger frequency dispersion for the improper ferroelectrics compared to a proper ferroelectric such as $PbTiO_3$. It is concluded that the primary structural order parameter controls the switching dynamics of such improper ferroelectrics.

Prototypical "proper" ferroelectrics such as $BaTiO_3$ (BTO), $PbZr_{1-x}Ti_xO_3$ (PZT), and $PbTiO_3$ (PTO) have been intensively studied for several decades for applications such as piezoelectric devices and non-volatile random-access memories (FE-RAMs).[1–3]

Prof. P. Barrozo
Physics Department
Federal University of Sergipe
São Cristóvão, Sergipe 49100-000, Brazil
E-mail: pbs@ufs.br

Prof. P. Barrozo, Dr. Y.-L. Tang, Dr. B. Prasad, S. Saremi, R. Ozgur, Dr. V. Thakare, Prof. L. W. Martin, Prof. R. Ramesh
Department of Materials Science and Engineering and Department of Physics
University of California
Berkeley, CA 94720, USA
E-mail: rramesh@berkeley.edu

Prof. P. Barrozo, Dr. Y.-L. Tang, Prof. L. W. Martin, Prof. R. Ramesh
Materials Sciences Division
Lawrence Berkeley National Laboratory
Berkeley, CA 94720, USA

D. R. Småbråten, Prof. S. M. Selbach
Department of Materials Science and Engineering
NTNU Norwegian University of Science and Technology Norway

R. A. Steinhardt, Dr. M. E. Holtz, Prof. D. G. Schlom Department of Materials Science and Engineering
Cornell University
Ithaca, NY 15805, USA

Dr. V. A. Stoica
Department of Materials Science and Engineering Pennsylvania State University
University Park, PA 16802, USA

In such proper ferroelectrics, the spontaneous polarization is the primary order parameter emerging from the transition to a ferroelectric state at the Curie temperature T_C. Many of the applications for such materials rely on there being sufficient field-driven evolution of polarization and mobility of the ferroelectric domain walls to enable polarization switching. Defects, such as oxygen vacancies, are generally considered to be detrimental to ferroelectric properties and are often key causes for reduced switchable polarization (via the pinning of domain walls), fatigue, imprint, and pinched ferroelectric hysteresis loops.[4]

The polar order in improper ferroelectrics, on the other hand, is a secondary effect coupled to a primary-order parameter that is often a structural distortion. In the improper ferroelectric hexagonal manganites h-$R$$MnO_3$ (R = Sc, Y, In, Ho, Lu) the polarization has a tri-linear coupling to the primary structural-order parameter. The improper ferroelectric hexagonal $LuFeO_3$ (h-LFO) is iso-structural with h-$RMnO_3$ and is also an improper ferroelectric with a $T_C \approx 1020$ K and antiferromagnetic Neel temperature $T_N \approx 150$ K.[5,6] While polarization switching has been extensively studied for proper ferroelectric perovskites,[7–11] little is known about switching in the improper ferroelectrics, let alone the role of point defects on the domain-wall dynamics and switching processes. In general, switching dynamics can be probed either in the time[12] or frequency domain (e.g., by probing the frequency-dependence of the coercive field or voltage) as a function of the ferroelectric layer thickness thus providing details about the domain nucleation and growth process.[13,14] The thickness (t) dependence of the coercive field has been classically described by interface nucleation and growth processes, first described by Kay and Dunn[15] in a model that predicts a $t^{-2/3}$ dependence of the coercive field. Numerous studies on thin films of proper ferroelectrics have validated, at least empirically, this model over thicknesses ranging from a few nanometers to several millimeters.[16–21]

Thus, while the switching dynamics of proper ferroelectrics is generally well established, a corresponding understanding of improper ferroelectrics such as h-LFO is missing, possibly because there are not as many exemplars of improper ferroelectrics. Since the polar order is a consequence of the primary structural distortion, one would intuitively expect a strong convolution of structural effects in the switching process. Given the

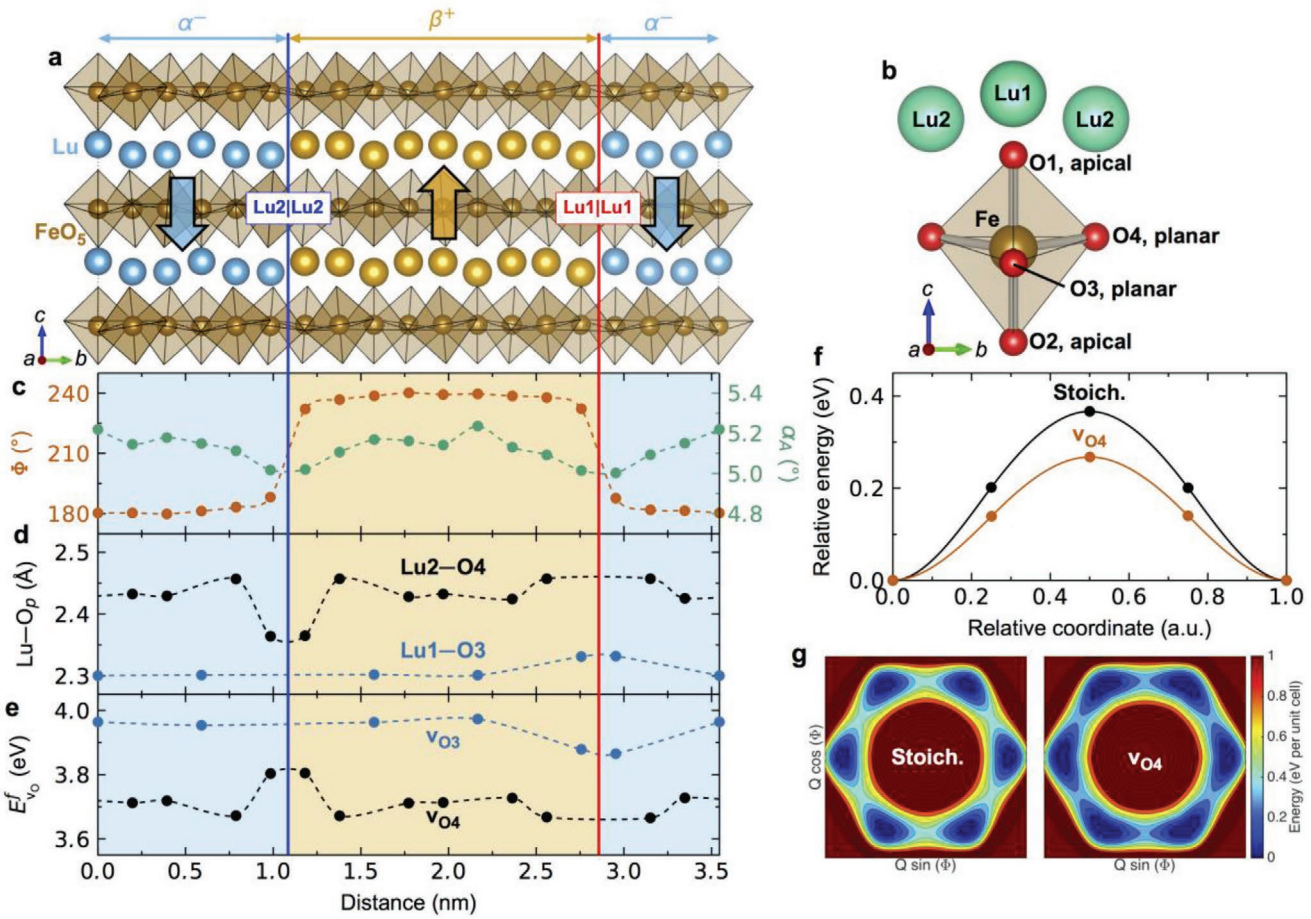

Figure 1. Interaction of neutral ferroelectric domain walls with oxygen vacancies. a) Supercell for DFT calculations including two neutral domain walls (blue and red are terminated by Lu2 and Lu1, respectively). b) Illustration of FeO_5 trigonal bipyramid and symmetry-inequivalent O and Lu positions. c) Calculated order parameter amplitude Q and phase Φ across the stoichiometric supercell in (a). Q is here represented by the FeO_5 trigonal bipyramid tilt angle α_A with respect to the ab-plane, while the azimuthal phase φ refers to the angle of the trimerization distortion. Dashed lines are guides to the eye. d) Calculated Lu–Op bond lengths across the supercell, illustrating the local strain fields near the two walls. e) Formation energies of vacancies of type O3 and O4, as illustrated in (b) at different positions across the supercell shown in (a). The Lu1 and Lu2 terminated walls are not equivalent because of different coordination environments at these walls (see Supporting Information). Dashed lines are guides to the eye. f) Calculated domain wall migration energy barriers for Lu2 terminated wall in the absence and presence of an O4 oxygen vacancy. g) Approximated "Mexican-hat" free energy landscape for $LuFeO_3$ with and without an O4 oxygen vacancy. Dashed lines in (c–e) are guides to the eye.

lack of a detailed understanding of the polarization dynamics in such improper ferroelectrics, we have initiated a comprehensive study of the same. Here, we study this switching process in epitaxial thin films of h-LFO, with particular attention to the influence of the oxygen (non-)stoichiometry through a combination of ab initio calculations and controlled synthesis coupled with detailed frequency-dependent studies of the switching field.

The unit cell of the hexagonal ferrites (h-$RFeO_3$) has four layers: two FeO layers and two LuO_2 layers where the lutetium cations are displaced along the c axis in a two-up/one-down corrugated pattern (**Figure 1**a). In the Fe–O layers, the iron cations are surrounded by five oxygens (three in the same plane as the iron and one above and below that layer), forming FeO_5 trigonal bipyramids.[22] The FeO_5 polyhedra share corners in the a–b plane and are separated by layers of lutetium (Figure 1a,b). The structural shift of the lutetium-layer relative to the Fe–O layers breaks inversion symmetry and is responsible for the improper ferroelectricity, resulting in a saturation polarization of ≈6 μC cm^{-2} at room temperature.[23] The Lu–O_2 and Fe–O layers are linked through the out-of-plane Lu–O bonds along the polar axis, while the lutetium cations are surrounded by eight oxygen ions (six in the same plane as the Lu–O_2 layers and one above and below that layer) forming LuO_8 polyhedra. The FeO_5 trigonal bipyramids are also rotated about the [120], which is responsible for the broken inversion symmetry of the h-$LuFeO_3$ structure, allowing for the emergence of ferroelectric order.[24] Similar to $YMnO_3$,[25–27] h-LFO is expected to be able to accommodate large oxygen nonstoichiometry.

First-principles calculations (see Computational Details in the Experimental Section) show that, as in $YMnO_3$, planar oxygen vacancies (O3 and O4, Figure 1b) are strongly favored over apical (O1 and O2)[28] (Supporting Information). To investigate the interplay between oxygen vacancies and ferroelectric domain walls in h-LFO, density functional theory (DFT) calculations were performed on supercells with two neutral domain walls, one Lu1 and one Lu2 terminated (Figure 1a). The

evolution of the crystal structure across the domain wall, represented by the order-parameter phase φ and amplitude Q, quantified by the FeO_5 planar tilt angle Φ and the apical tilt angle α_P relative to the [001], respectively (Figure 1c), is similar to that of isostructural $YMnO_3$.[29]

At neutral domain walls there is no internal electric field that can drive accumulation or depletion of oxygen vacancies; only elastic strain fields arising from the discontinuity in the structural order parameter across the walls can drive defect accumulation or segregation. To visualize the local nature of such elastic strain fields the bond lengths between the lutetium cations and planar oxygen are shown (Figure 1d), from which it is also evident that the local environments at Lu1- and Lu2-terminated walls differ (Supporting Information); a feature that is also found for domain walls in h-$R$$MnO_3$ systems.[30] In contrast with proper ferroelectrics, the calculations show that oxygen vacancies should not accumulate at the domain walls. While the energy of oxygen vacancy in site O3 (see Figure 1d,e) (v_{O3}) are found to be more stable at Lu1-terminated walls, the oxygen vacancy in site O4 (v_{O4}) are more stable in the bulk of a domain than at the Lu2-terminated walls. As v_{O4} are 0.25 eV lower in energy than v_{O3}, the oxygen vacancies are expected to have sufficient mobility to reach their most stable positions during post-synthesis cooling. Only v_{O4} is considered in the following analysis.

To address the impact of oxygen vacancies on the macroscopic ferroelectric response, climbing-image nudged elastic band (Ci-NEB) calculations were done to quantify the domain-wall-migration energy barrier in the presence and absence of oxygen vacancies. We find that an oxygen vacancy reduces the domain-wall-migration energy barrier by ≈27% from 0.37 eV in stoi-chiometric materials to 0.27 eV in the presence of a v_{O4} vacancy (Figure 1f). Macroscopically, this implies that the coercive field should be smaller in oxygen-deficient h-LFO than in stoichio-metric versions, as the energy barrier for switching the polariza-tion is reduced, as illustrated by the flattened energy landscape in the brim of the approximated Mexican-hat potential (Figure 1g).

With this theoretical framework as the background, we next focus on experimental results which show that the oxygen-defect chemistry (and thus the switching characteristics) of the h-LFO thin film can be systematically controlled during growth: 1) by annealing in different oxygen pressures and 2) by varying the frequency of the laser pulses and thus the deposition rate (details of the deposition process are presented, Experimental Section.). We used an epitaxial top and bottom layer of tin-doped indium oxide (ITO) that promotes (001)-oriented epitaxial growth of the h-LFO, as evidenced by the lack of any other crystallographic orientations from X-ray diffraction studies (**Figure 2**a) as well as reciprocal space maps (RSMs,

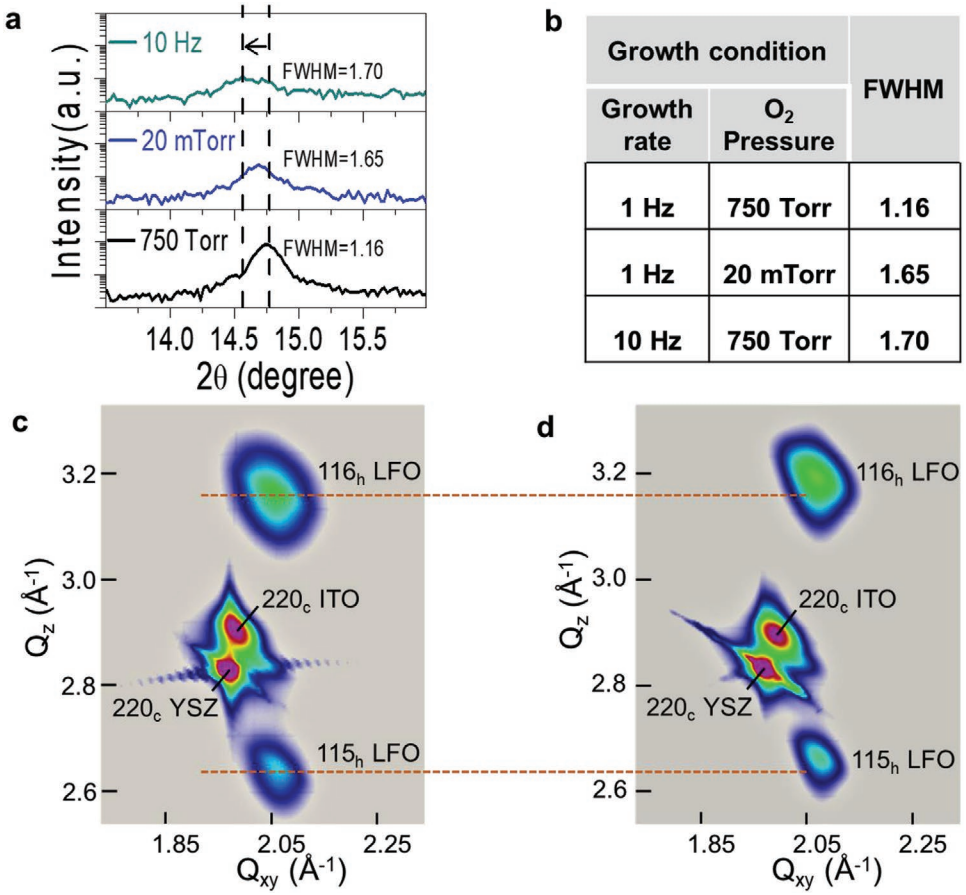

Figure 2. a) X-ray diffraction of the (002) peak of 60 nm thick h-LFO thin film produced by pulsed laser deposition (PLD) and grown at 10 Hz (cooled in 750 Torr of O_2), grown at 1 Hz and cooled in 750 Torr O_2 and cooled in 20 mTorr of O_2. b) Table to show the full width at half maximum (FWHM) of films grown under different conditions. c,d) Reciprocal space maps of samples cooled at 750 Torr and 20 mTorr, respectively.

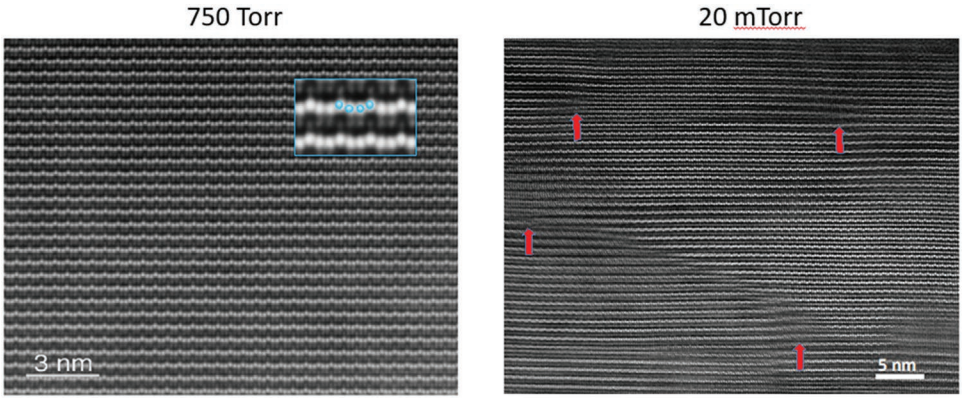

Figure 3. a) HRSTEM of defect-free structure in 750 Torr sample; b) HRSTEM of defects in 20 mTorr sample.

Figures 2c,d). The reduction of intensity in the (002) peak of h-LFO grown in different conditions (Figure 2a) can be attributed to the creation of oxygen vacancies related by the changing the oxygen pressure during cooling or the laser repetition rate at growth. The shift of the (002)-diffraction peak toward lower Bragg angles with less oxidizing conditions and higher deposition frequency indicates an increase of the out-of-plane lattice parameter, similar to that reported for the $YMnO_3$.[31] The full-width-at-half-maximum (FWHM) of films grown under different conditions (growth pressures and laser repetition rates) indicate that the crystallinity of the h-LFO films can be tuned by changing the oxygen annealing pressure or by controlling the deposition rate during the growth (Figure 2b). RSMs for the h-LFO heterostructures grown with optimal conditions by PLD reveal good epitaxy for the 60-nm-thick films annealed at 750 Torr (Figure 2c) and 20 mTorr (Figure 2d) of oxygen.

High-resolution scanning transmission microscopy (HR-STEM) studies provide a direct, microscopic picture of defects and local structural changes. The optimally cooled (750 Torr of oxygen) heterostructures show a highly ordered structure; the trimerization structure of one-up/two-down cations can also be observed (zoom-in, **Figure 3**a). The samples cooled in 20 mTorr of oxygen (Figure 3b) and the sample grown at faster deposi-tion rates 10 Hz both show a higher density of stacking defects when compared with samples prepared under optimal growth conditions shown in Figure 3a. At higher resolution, these defects are resolved to be a mixture of stacking defects, illustrated in the HR-STEM images (Figure S3a,b, Supporting Information). The disturbed region, where a continuous increase of the vertical coordinates is illustrated in Figure S3c, Supporting Information. This defect is characterized by a change in the stacking sequence from 2UP/1DOWN or 1UP/2DOWN (where the UP/DOWN correspond to the shifts of the Lu atom positions along the *c*-axis) in the perfect crystal to one in which the stacking sequence is changed to 1UP/1MIDDLE/1DOWN, that is, resembling a "1–2–3" staircase.

We now turn to detailed ferroelectric measurements. In order to explore (and reduce) the influence of leakage, the measurements were carried out at both 100 and 300 K (ferroelectric hysteresis loops completed at 300 K are shown in Figure S4, Supporting Information). The leakage current at 100 K (Figure S5, Supporting Information) is small enough to allow us to investigate the polarization switching behavior across a wide frequency range (i.e., from 50 mHz to 125 kHz—nearly six orders of magnitude). The ferroelectric hysteresis loops for three representative h-LFO samples, at a fixed frequency of 25 kHz, are provided for comparison (**Figure 4**a–c). The corresponding frequency dependence is also provided in Figure S6, Supporting Information. The first key observation is that all samples show well-saturated hysteresis loops at 100 K.

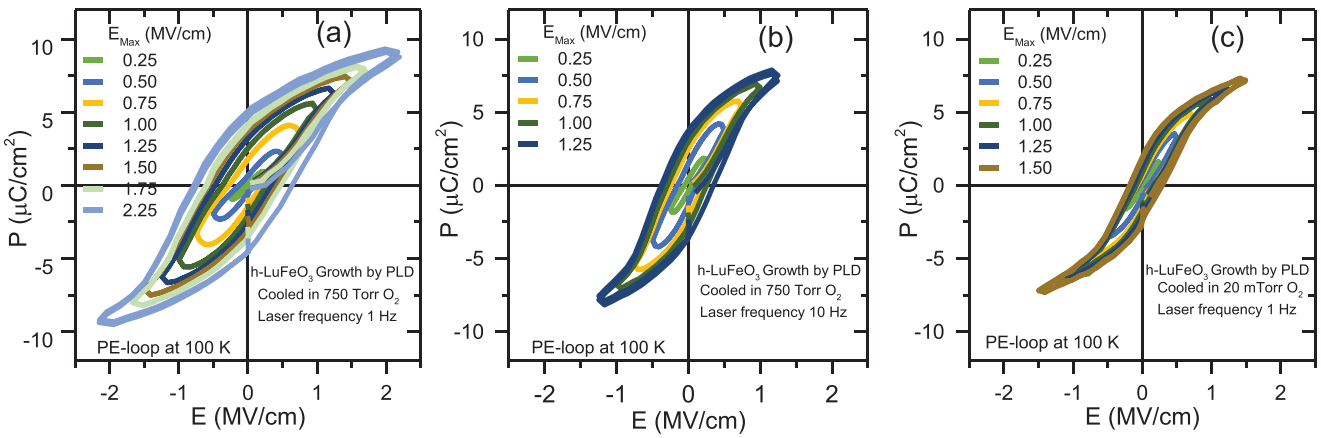

Figure 4. a–c) Ferroelectric hysteresis loops of the four Pt/ITO/LFO/ITO model systems used in this study at 100 K: a) grown at a deposition rate of 1 Hz, cooled in 750 Torr of oxygen; b) grown at 10 Hz and cooled in 750 Torr of oxygen; c) grown at 1 Hz and cooled in 20 mTorr of oxygen.

An interesting feature is that the coercive field is progressively reduced by the introduction of defects during growth, both by depositing an order of magnitude faster (PLD growth at 10 Hz versus 1 Hz; Figure 4a,b, respectively) or by cooling the film in a less oxidizing environment (PLD growth at 1 Hz and cooled in 20 mTorr versus 750 Torr; Figure 4a,c, respectively). This reduction of coercive field with increase in defect concentration is consistent with our theoretical finding that oxygen vacancies reduce the domain-wall-migration barrier.

Next we explored the role of the changing growth conditions on the frequency dependence of the coercive field. For classical ferroelectrics, the Ishibashi & Orihara model[13] describes the dynamics of the domain walls under the influence of either an AC or pulsed external field. The domain-wall velocity is a func-tion of only the applied field E (i.e., $v(E,t)$) and the volume of the domain switching at a time t is described as a power law function of switching time. In the frequency domain, a variant of this model relates the coercive field obtained from a polari-zation-electric field hysteresis loop to the test frequency which can be described by: $E_c = E_{c,0} + a f^{b}$, where f is the measurement frequency, $E_{c,0}$ is the limiting value of the switching field (i.e., the quasi-static switching field at zero frequency $E_{c,0}$), and a and b are obtained from fits to the frequency dependent data. The frequency dependence of the coercive field is captured through the exponent "b." To eliminate the effects of small shifts of the hysteresis loops (for example, due to internal fields), we have plotted the average coercive field ($[E_c^+ - (-E_c^-) = 2E_c]/2$) versus frequency. The frequency dependence of this average coercive field was extracted from the ferroelectric hysteresis loops for at least 20 capacitors on each sample and for multiple samples for each growth condition. We plot the coercive field as a function of log(f) for all samples (**Figure 5**). For comparison, we include data for $PbTiO_3$ as a representative proper ferroelectric. The data were fitted using the Ishibashi model (solid lines, Figure 5). The data for each of the samples fits well to this model (with regression coefficients in the 0.93–0.99 range), albeit with significantly different exponents, which we explain next.

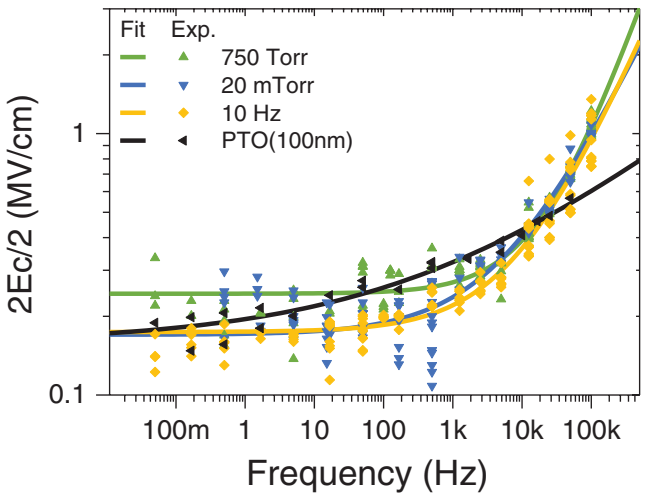

Figure 5. Coercive field as a function of frequency for LFO samples grown at different conditions and for PTO. The solid lines are fits to the experimental data using a power law described by the Ishibashi model.

Table 1. Quasi-static coercive field, $E_{c,0}$, and the frequency dispersion exponent, b, obtained from the fit using the Ishibashi model to describe the mechanism to sweep the polarization for different samples of h-LFO compared with PTO (proper ferroelectrics).

Sample	$E_{c,0}$ [kV cm^{-1}]	b
750 Torr	244	0.77
20 mTorr	170	0.59
10 Hz	174	0.61
PTO	158	0.22

There are several key observations from this frequency-dependent data (summarized in **Table 1**). First, as expected, all of the samples show a frequency dependence of the coercive field—that of the proper ferroelectric ($PbTiO_3$) can be fitted well to a power law behavior with an exponent of $b \approx 1/4$; this is con-sistent with previous reports.[9,32] Second, as we already observed in the ferroelectric hysteresis loops (Figure 4), the defective h-LFO samples show a lower $E_c(0)$ (by ≈40%) as compared to PLD samples cooled in 750 Torr of oxygen. Most importantly, however, the value of the exponent b for all of the h-LFO sam-ples is ≈0.66. To get a more unified picture, we have normalized the average coercive field by plotting $[E_c - E_c^0/a]$ as a function of frequency (Figure S7, Supporting Information). The frequency dispersion for the proper ferroelectric ($PbTiO_3$) can be fitted well with a slope of ≈1/4. In contrast, the improper ferroelec-tric samples discussed herein have a large slope of ≈2/3 for all samples studied here. Thus, from the data (Figure 5; Figure S7, Supporting Information), we observe a clear difference in switching dynamics between the improper (h-LFO) and proper (PTO) ferroelectrics.

Propelled by this observation as well as the significantly different exponent in the frequency dispersion of the coercive field compared to single crystals of the sister compound, $ErMnO_3$ (0.66 for epitaxial $LuFeO_3$ thin films versus ≈0.10 for the single crystal of $ErMnO_3$),[33] we proceeded to study the thickness dependence of this frequency dispersion. We note that prac-tical limitations in the synthesis of thin films (i.e., extended growth times of over a few hours) limited us to thicknesses of up to 300 nm. The frequency dispersion behavior (with fre-quencies ranging from 0.1 Hz to 125 kHz) from this thickness series (5 to 300 nm) is shown in **Figure 6**a, from which we have extracted the $E_c(0)$ and "b" (the exponent in the frequency dispersion). They are shown in Figure 6b as a function of thick-ness; the dotted curves in Figure 6b are exponential fits to the actual data and the fitting equations are provided in the figure caption. The thickness-dependent data reveals some interesting insights into the switching behavior of the thin film compared to the crystals.[33] First, the exponent, b, appears to be asymp-toting to a value of ≈0.4–0.5 in the thin film case. The thickness dependence of the films deposited with a higher concentration of oxygen vacancies (20mTorr) also shows a similar thickness dependence, with the exponent asymptoting to a value of ≈0.5 (for the sake of simplicity, we have not included that data here).

Furthermore, similar measurements on epitaxial $LuFeO_3$ films with epitaxial Ir top and bottom electrodes reveal a similar trend in the b-value.[34]

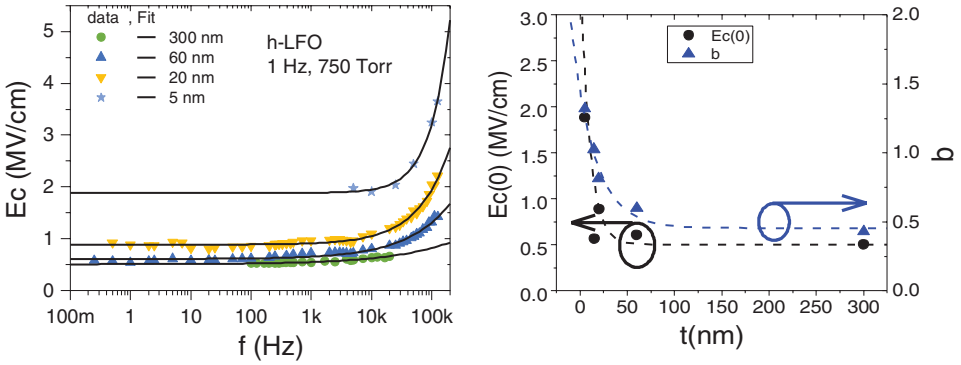

Figure 6. a) Coercive field as a function of frequency for LFO samples with varying thickness. The solid lines are fits to the experimental data using a power law described by the Ishibashi model. b) Thickness dependence of the $E_c(0)$ and the exponent, b. The blue dotted curve is an exponential fit of the exponent b with the equation $b = \exp(-x/24) + 0.45$, the black dotted curve is guide to the eye.

One broad conclusion that we can come to is that the $E_c(0)$ can be manipulated significantly through defects in the LFO or the contact electrode, but the exponent in the frequency dispersion of the switching field appears to be similar for thin films. This is significantly different from that of the crystals, thus pointing to some fundamental differences in the switching behavior in thin films that are tethered to a substrate which imposes a mechanical constraint to the deformability of the thin film. Specifically, for a proper ferroelectric, all energy from the external applied field is used to move the DWs and change the polarization. In contrast, for an improper ferroelectric a large portion of the energy is spent on overcoming the structural distortion in the crystal, that is, move the atoms to rotate the polyhedra, and the balance is available to change the polarization direction.

Another difference between proper ferroelectric perovskites such as $PbTiO_3$ and the improper ferroelectric h-LFO is the interaction between oxygen vacancies and domain walls. While it is well established, both from experiments[35,36] and recent DFT studies,[37–44] that oxygen vacancies segregate to and pin ferroelectric domain walls, this is not the case for improper ferroelectrics like h-LFO and $YMnO_3$.[28,29] Following the extension of the coupling diagram for primary ferroic orders[45] to also include electrochemistry and stoichiometry,[46] our results demonstrate a strong and positive coupling between ferroelectricity and the chemical potential as a conjugate field. For defects that also give rise to enhanced conductivity, there may be an optimal concentration of defects which reduced the coercive field without causing significant leakage current. Our finding that the presence of an oxygen vacancy reduces the domain-wall-migration barrier opens the possibility of tuning the coercive field through oxygen-vacancy concentration by growth conditions, or even to "reconfigure" a device by post-synthesis annealing. To utilize oxygen stoichiometry to tune the coercive field is particularly promising for improper ferroelectrics where the polarization is less sensitive to point defects[26,28] than conventional perovskites where polarization is the primary order parameter.

In summary, we have examined the coupling between growth condition, crystal defects, and polarization switching dynamics in a model "improper" ferroelectric, $LuFeO_3$. There are four key implications from this work. First, the quasi-static switching field can be changed by controlling the defect structure of LFO through growth parameters. Second, in contrast with the proper ferroelectric perovskites $PbTiO_3$, defects reduce the switching field in LFO. This is supported by DFT calculations showing that oxygen vacancies reduce the domain wall migration energy barrier. Third, the frequency dispersion studies of a large number of LFO films as well as PTO films show a universal power dependence of the coercive field on the measurement frequency. Fourth, the exponent of this power dependence is significantly higher for LFO compared to PTO, indicating a key role of the primary structural order parameter on the energetics of the polarization switching.

Experimental Section

Sample Preparation: ITO/h-LFO/ITO heterostructure growth: Epitaxial (20 nm) ITO/(60 nm) h-LFO/(20 nm) ITO were grown on (111) oriented single crystal of 9.5% yttria-stabilized zirconia substrates by pulsed-laser deposition (PLD) using a KrF excimer laser (λ = 248 nm). 20 nm of ITO was used as top and bottom electrode grown at 920K with a laser fluence ≈4.5 J cm^{-2} and laser repetition rate of 2 Hz with an oxygen partial pressure of 50 mTorr. 60 nm of hexagonal $LuFeO_3$ (h-LFO) was grown using a laser fluence of 3.8 J cm^{-2}, partial oxygen pressure of 20 mTorr, 1090 K, and laser repetition rate ranging from 1 Hz to 10 Hz. All three-layer ITO/LFO/ITO was grown in situ, using a base pressure above 1×10^{-6} Torr. After deposition of the ITO top-layer the ITO/h-LFO/ITO heterostructure was annealed at 1120 K and with different O_2 partial pressures ranging from 20 mTorr to 750 Torr. The density of the structural defects on the h-LFO was induced and controlled by change the laser repetition rate of the LFO layers and by change the partial oxygen pressure on the cooling chamber after the annealing. Capacitor with different diameter sizes were produced by photolithography followed by ion-milling processes. Before the ion milling process a 20 nm platinum layer was grown on the structure by sputtering.

Sample Characterization: The structural properties were investigated by X-ray diffraction (XRD) and reciprocal space map (RSM) using a Panalytical X'Pert^3 MRD. The microstructure of the Pt/ITO/h-LFO/ITO/YSZ(111) was characterized by high-resolution transmission electron microscopy and atomic force microscopy (show in Figure S2d, Supporting Information). The ferroelectric loops were measured using a Radiant Technologies Precision Multiferroic system attached to a Lake Shore probe station at temperatures between 100 and 300 K. Ferroelectric hysteresis loops were measured at different frequencies and voltage drive amplitude. We used at least 20 capacitors to perform the analyses for each frequency and drive amplitude.

Computational Details: DFT calculations were carried out with VASP[47,48] using PBEsol[49] and the Lu_3, Fe, and and O pseudopotentials. A cutoff of 550 eV was used along with an effective $U - J = 3.5$ eV applied to Fe 3d.[50] A frustrated ferromagnetic (f-AFM) order[51] on the Fe sublattice was assumed. A Γ-centered 2 × 2 × 2 k-point mesh was used for (2 × 2 × 1) supercells with one oxygen vacancy and ions were relaxed until the forces were below 0.005 eV Å^{-1}. The oxygen vacancy formation energy in neutral cells was calculated as $E^f = E_{def} - E_{ref} + \mu_O$ where E_{def} and E_{ref} are the total energies of the oxygen defect cell and the stoichiometric cell, respectively. The chemical potential of oxygen, μ_O, was set to $\mu_O = -5$ eV, corresponding to typical conditions for PLD.

The structural evolution across domain walls were studied using a (1 × 6 × 1) supercell[52] with two parallel domain walls ≈18 Å apart and ions were relaxed to forces below 0.01 eV Å^{-1}. Interactions between domain walls and oxygen vacancies were studied using (2 × 6 × 1) supercells and ions were relaxed to forces below 0.01 eV Å^{-1}. Segregation enthalpies ΔE_{seg} for the two planar oxygen vacancy sites O3 and O4 were determined by their formation energy profiles across the supercell. Domain wall migration energy barriers were calculated with the climbing-image nudged elastic band (Ci-NEB) method.[53,54] The walls were assumed to migrate as parallel equidistant walls, using five intermediate images and with forces on ions relaxed to 0.03 eV Å^{-1}. The free-energy landscape was determined from energy barriers between the domains in using Ci-NEB as described above, and from the static energy landscape of the $K_3 + \Gamma^-_2$ mode amplitude in (2 × 2 × 1) supercells using intermediate structures interpolated between $P6_3/mmc$ and $P6_3cm$ structures with and without oxygen vacancies.

Acknowledgements

The authors acknowledge Professor Nicola Spaldin for helpful discussions. D.R.S. and S.M.S. were supported by the Research Council of Norway (Project no. 231430). The work at Berkeley (P.B. & R.R.) was supported by the SRC ASCENT project, which is part of the SRC-JUMP program. Computational resources were provided by UNINETT Sigma2 through Projects NN9264K and ntnu243. P.B. was funded in part by the Coordenação de Aperfeiçoamento de Pessoal de Nível Superior—Brasil (CAPES) (process no. 88881.119454/2016-01)—Finance Code 001. S.S. acknowledges support from the U.S. Department of Energy, Office of Science, Office of Basic Energy Sciences, under Award Number DE-SC-0012375 for the development and study of ferroelectric thin films. L.W.M. acknowledges the support of the National Science Foundation under Grant DMR-1708615. The work at Cornell (R.A.S., M.E.H., and D.G.S.) was supported by ASCENT, one of six centers in JUMP, a Semiconductor Research Corporation (SRC) program sponsored by DARPA.

Conflict of Interest

The authors declare no conflict of interest.

Keywords

ferroelectricity, h-LFO, $LuFeO_3$, multiferroics

[1] V. Garcia, S. Fusil, K. Bouzehouane, S. Enouz-Vedrenne, N. D. Mathur, A. Barthelemy, M. Bibes, *Nature* **2009**, *460*, 81.
[2] M. Okuyama, Y. Hamakawa, *Ferroelectrics* **1985**, *63*, 243.
[3] S. Trolier-McKinstry, P. Muralt, *J. Electroceram.* **2004**, *12*, 7.
[4] M. E. Lines, A. M. Glass, *Principles and Applications of Ferroelectrics and Related Materials*, Clarendon, Oxford, UK **1977**.
[5] T. Katsufuji, M. Masaki, A. Machida, M. Moritomo, K. Kato, E. Nishibori, M. Takata, M. Sakata, K. Ohoyama, K. Kitazawa, H. Takagi, *Phys. Rev. B* **2002**, *66*, 134434.
[6] T. Katsufuji, S. Mori, M. Masaki, Y. Moritomo, N. Yamamoto, H. Takagi, *Phys. Rev. B* **2002**, *64*, 104419.
[7] W. Merz, *Phys. Rev.* **1954**, *95*, 690.
[8] D. J. Jung, M. Dawber, J. F. Scott, L. J. Sinnamon, J. M. Gregg, *Integr. Ferroelectr.* **2002**, *48*, 59.
[9] J. F. Scott, *Integr. Ferroelectr.* **1996**, *12*, 71.
[10] P. Chandra, M. Dawber, P. B. Littlewood, J. F. Scott, *Ferroelectrics* **2004**, *313*, 7.
[11] P. Gao, C. T. Nelson, J. R. Jokisaari, S.-H. Baek, C. W. Bark, Y. Zhang, E. Wang, D. G. Schlom, C.-B. Eom, X. Pan, *Nat. Commun.* **2011**, *2*, 591.
[12] J. Li, B. Nagaraj, H. Liang, W. Cao, *Appl. Phys. Lett.* **2004**, *84*, 1174.
[13] Y. Ishibashi, H. Orihara, *Integr. Ferroelectr.* **1995**, *9*, 57.
[14] A. K. Tagantsev, L. E. Cross, J. Fousek, *Domains in Ferroic Crystals and Thin Films*, Springer-Verlag, New York **2010**.
[15] H. F. Kay, J. W. Dunn, *Philos. Mag.* **1962**, *7*, 2027.
[16] S. Ren, C. Lu, J. Liu, H. Shen, Y. Wang, *Phys. Rev. B* **1996**, *54*, R14337.
[17] J. F. Scott, *J. Phys.: Condens. Matter* **2006**, *18*, R361.
[18] M. Dawber, P. Chandra, P. B. Littlewood, J. F. Scott, *J. Phys.: Condens. Matter* **2003**, *15*, L393.
[19] J. F. Scott, M. Dawber, A. Q. Jiang, F. D. Morrison, *Ferroelectrics* **2003**, *286*, 223.
[20] P. Maksymovych, M. Huijben, M. Pan, S. Jesse, N. Balke, Y. H. Chu, H. J. Chang, A. Y. Borisevich, A. P. Baddorf, G. Rijnders, D. H. A. Blank, R. Ramesh, S. V. Kalinin, *Phys. Rev. B* **2012**, *85*, 014119.
[21] O. Trithaveesak, J. Schubert, C. Buchal, *J. Appl. Phys.* **2005**, *98*, 114101.
[22] X. Xu, W. Wang, *Mod. Phys. Lett. B* **2014**, *28*, 1430008.
[23] Y. K. Jeong, J.-H. Lee, S.-J. Ahn, H. M. Jang, *Chem. Mater.* **2012**, *24*, 2426.
[24] H. Das, A. L. Wysocki, Y. Geng, W. Wu, C. J. Fennie, *Nat. Commun.* **2014**, *5*, 2998.
[25] C. J. Fennie, K. M. Rabe, *Phys. Rev. B* **2005**, *72*, 100103.
[26] S. H. Skjærvø, E. T. Wefring, S. K. Nesdal, N. H. Gaukås, G. H. Olsen, J. Glaum, T. Tybell, S. M. Selbach, *Nat. Commun.* **2016**, *7*, 13745.
[27] Y. Du, X. Wang, D. Chen, Y. Yu, W. Hao, Z. Cheng, S. X. Dou, *Phys. Chem. Chem. Phys.* **2013**, *15*, 20010.
[28] S. H. Skjærvø, D. R. Småbråten, N. A. Spaldin, T. Tybell, S. M. Selbach, *Phys. Rev. B* **2018**, *98*, 184102.
[29] J. Schaab, S. H. Skjærvø, S. Krohns, X. Dai, M. E. Holtz, A. Cano, M. Lilienblum, Z. Yan, E. Bourret, D. A. Muller, M. Fiebig, S. M. Selbach, D. Meier, *Nat. Nanotechnol.* **2018**, *13*, 1028.
[30] D. R. Småbråten, Q. N. Meier, S. H. Skjærvø, K. Inzani, D. Meier, S. M. Selbach, *Phys. Rev. Mater.* **2018**, *2*, 114405.
[31] A. J. Overton, J. L. Best, I. Saratovsky, M. A. Hayward, *Chem. Mater.* **2009**, *21*, 4940.
[32] H. Orihara, S. Hashimoto, Y. Ishibashi, *J. Phys. Soc. Jpn.* **1994**, *63*, 1031.
[33] A. Ruff, Z. Li, A. Loidl, J. Schaab, M. Fiebig, A. Cano, Z. Yan, E. Bourret, J. Glaum, D. Meier, S. Krohns, *Appl. Phys. Lett.* **2018**, *112*, 182908.
[34] R. A. Steinhardt, M. E. Holtz, P. Barrozo da Silva, Z. Xiao, R. Ozgur, D. A. Tenne, R. N. Candler, D. A. Muller, P. Shafer, E. Arenholz, J. A. Mundy, R. Ramesh, D. G. Schlom, *unpublished*.

[35] S. Aggarwal, R. Ramesh, *Annu. Rev. Mater. Sci.* **1998**, *28*, 463.
[36] M. Dawber, J. F. Scott, *Appl. Phys. Lett.* **2000**, *76*, 1060.
[37] L. He, D. Vanderbilt, *Phys. Rev. B* **2003**, *68*, 134103.
[38] A. Chandrasekaran, X.-K. Wei, L. Feigl, D. Damjanovic, N. Setter, N. Marzari, *Phys. Rev. B* **2016**, *93*, 144102.
[39] A. Chandrasekaran, D. Damjanovic, N. Setter, N. Marzari, *Phys. Rev. B* **2013**, *88*, 214116.
[40] C. Paillard, G. Geneste, L. Bellaiche, B. Dkhil, *J. Phys.: Condens. Matter* **2019**, *29*, 485707.
[41] T. Xu, T. Shimada, Y. Araki, J. Wang, T. Kitamura, *Nano Lett..* **2016**, *16*, 454.
[42] X. Y. Li, Q. Yang, J. X. Cao, L. Z. Sun, Q. X. Peng, Y. C. Zhou, R. X. Zhang, *J. Phys. Chem. C* **2018**, *122*, 3091.
[43] S. Farokhipoor, C. Magén, S. Venkatesan, J. Íñiguez, C. J. M. Daumont, D. Rubi, E. Snoeck, M. Mostovoy, C. de Graaf, A. Müller, M. Döblinger, C. Scheu, B. Noheda, *Nature* **2014**, *515*, 379.
[44] J. J. Gong, C. F. Li, Y. Zhang, Y. Q. Li, S. H. Zheng, K. L. Yang, R. S. Huang, L. Lin, Z. B. Yan, J.-M. Liu, *Mater. Today Phys.* **2018**, *6*, 9.
[45] N. A. Spaldin, M. Fiebig, *Science* **2005**, *309*, 391.
[46] S. V. Kalinin, N. A. Spaldin, *Science* **2013**, *341*, 858.
[47] G. Kresse, J. Furthmüller, *Phys. Rev. B* **1996**, *54*, 11169.
[48] G. Kresse, D. Joubert, *Phys. Rev. B* **1999**, *59*, 1758.
[49] J. P. Perdew, A. Ruzsinszky, G. I. Csonka, O. A. Vydrov, G. E. Scuseria, L. A. Constantin, X. Zhou, K. Burke, *Phys. Rev. Lett.* **2008**, *100*, 136406.
[50] S. L. Dudarev, G. A. Botton, S. Y. Savrasov, C. J. Humphreys, A. P. Sutton, *Phys. Rev. B* **1998**, *57*, 1505.
[51] J. E. Medvedeva, V. I. Anisimov, M. A. Korotin, O. N. Mryasov, A. J. Freeman, *J. Phys.: Condens. Matter* **2000**, *12*, 4947.
[52] Y. Kumagai, N. A. Spaldin, *Nat. Commun.* **2013**, *4*, 1540.
[53] G. Henkelman, B. P. Uberuaga, H. Jónsson, *J. Chem. Phys.* **2000**, *113*, 9901.
[54] G. Henkelman, H. Jónsson, *J. Chem. Phys.* **2000**, *113*, 9978.